General equivalent circuit for intermediate band devices: Potentials, currents and electroluminescence

A. Luque and A. Martí
Instituto de Energía Solar, Universidad Politécnica de Madrid, E.T.S.I. Telecomunicación, Ciudad Universitaria s/n Madrid, Madrid 28040, Spain

C. Stanley
Department of Electronics and Electrical Engineering, University of Glasgow, Glasgow G12 8QQ, United Kingdom

N. López and L. Cuadra
Instituto de Energía Solar, Universidad Politécnica de Madrid, E.T.S.I. Telecomunicación, Ciudad Universitaria s/n Madrid, Madrid 28040, Spain

D. Zhou and J. L. Pearson
Department of Electronics and Electrical Engineering, University of Glasgow, Glasgow G12 8QQ, United Kingdom

A. McKee
CST Global Ltd. B-7, Kelvin Campus, West of Scotland Science Park, Glasgow G20 0TH, United Kingdom

(Received 2 February 2004; accepted 23 April 2004)

A general model to describe the operation of intermediate band solar cells (IBSCs), incorporating a significant number of physical effects such as radiative coupling between bands, and impact ionization and Auger recombination mechanisms, is presented in equivalent circuit form. The model is applied to IBSC prototypes fabricated from InAs quantum dots structures to determine the value of the circuit elements involved. The analysis shows evidence of splitting between the conduction and intermediate band quasi-Fermi levels, one of the fundamental working hypotheses on which operation of the IBSC depends. The model is also used to discuss the limitations and potential of this type of cell. © *2004 American Institute of Physics.* [DOI: 10.1063/1.1760836]

I. INTRODUCTION

Intermediate band (IB) solar cells[1] have been proposed as a means of exploiting below-band-gap photons to generate additional current beyond that corresponding to band-to-band generation. Furthermore, in IB solar cells, the additional current produced by the absorption of these subgap photons is intended to be delivered at a voltage close to the semiconductor band gap and therefore, above the energy difference between either the IB level (or band) and the valence band (VB), or the IB level and the conduction band (CB).

There may be several mechanisms capable of promoting an electron from the VB to the CB via the intermediate band. Regardless of the mechanism, basic thermodynamic reasons[2] require that the global process of pumping an electron from the VB to the CB through the IB requires the absorption of two photons. The most obvious one[1] involves the absorption of two consecutive below-band-gap energy photons to induce a transition from the VB to the IB and from there, to the CB [processes labeled ''1'' and ''2'' in Fig. 1(a) to which the ordinary, single photon generation process ''3'' directly between the CB and the VB has been added]. Alternatively, an impact ionization mechanism,[3,4] in which the energy of an electron returning from the IB to the VB is used to pump another electron from the IB to the CB [as shown by process ''4'' in Fig. 1(a)] can also take place. Note that two photons are also needed in this case: one, as before, to pump an electron from the VB to the IB and another, to pump a second electron from the VB to the IB. Then, an electron from the IB can subsequently relax back to the VB, releasing its energy via impact ionization to an electron in the IB which is pumped to the CB. As anticipated, the net result of these processes, in the stationary state, is a single electron being pumped from the VB to the CB.

It is worth remembering that all the processes that are the reverse of those explicitly indicated in Fig. 1(a) (luminescent photon emission and Auger recombination) must coexist as required by detailed balance arguments.

The achievement of a high output voltage requires that three different quasi-Fermi levels appear in the excited material,[1] one each for both the VB and the CB, as in ordinary semiconductors, and one for the IB. The complete device is realized by sandwiching the IB material between two ordinary semiconductors without an IB, one *p* type and the other *n* type. This has been represented in Fig. 1(b) where the three quasi-Fermi levels, ϵ, have been labeled with the suffixes FC, FI, and FV to relate them to the electrons in the CB, IB, and VB respectively. The output voltage V_{CV} is related to the difference between the CB and VB quasi-Fermi levels at the *n* and *p* contacts respectively,

$$V_{VC}=\frac{\epsilon_{FC}-\epsilon_{FV}}{e}, \tag{1}$$

where *e* is the electron charge. The differences between

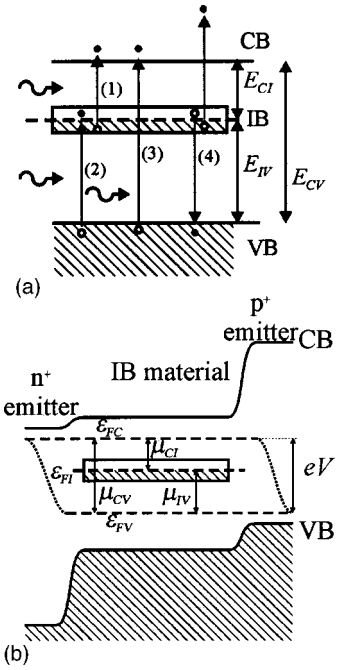

FIG. 1. (a) Simplified band-gap diagram including an intermediate band to show the different generation processes between bands. (b) Simplified band-gap diagram of a complete IBSC structure in which the IB material has been sandwiched between two emitters. Quasi-Fermi level splitting is also shown.

quasi-Fermi level pairs, $\epsilon_{FX}-\epsilon_{FY}$, are also the chemical potentials μ of the photons emitted by electroluminescence with the diode forward biased.

The maximum theoretical efficiency of an ideal IB solar cell is 63.2%, exceeding the 40.7% of ordinary single gap solar cells.[1]

In a series of papers,[3–7] several different phenomena in IB solar cells have been studied. In Sec. II, these are represented in equivalent circuit form. In Sec. III, experimental data obtained from the characterization of intermediate band solar cells (IBSCs) manufactured from InAs quantum dot structures is used to fit the parameters involved in the circuit description and to gather information about the performance of the IBSCs. Finally, conclusions are summarized in Sec. IV

II. INTERMEDIATE BAND SOLAR CELL EQUIVALENT CIRCUIT

The ideal model of the IBSC was initially described in Ref. 1. Later, the model was successively generalized to include elements of nonideality such as the existence of overlap between absorption coefficients[5–7] and the dual presence of impact ionization and Auger recombination phenomena.[3,4] Figure 2 represents all these combined effects in equivalent circuit form. In particular, the branches of the circuit labeled as *impact Auger* are the ones contributing when the above mentioned impact ionization and Auger mechanisms are present. All the elements of the circuit and their relationship to their physical origin are described in Table I.

The relation between the mathematical expression of some of the circuit elements and their corresponding physical models is not evident at first sight. The references given above should be consulted for the necessary details.

The treatment of Ref. 5 has been modified slightly to take into account room temperature illumination of the cell, previously ignored, given the inclusiveness of the reverse currents of the diodes appearing in the circuit.

A few additional comments are necessary to assist the comprehension of the elements described in Table I. Suffixes (a,b,c) or XY can take any one of the values CV, CI, and IV and refer to the transitions between the X band (conduction, intermediate, or valence) and the Y band.

Current through the diodes is assumed to be of the form

$$J_{XY}=J_{0,XY}\left(\exp\frac{eV_{YX}}{kT}-1\right), \tag{2}$$

where V_{YX} is the voltage difference between the circuit nodes across which the diode is connected. In the formulism given here, current refers to current density. The exponential form appearing in Eq. (2) reveals that the Boltzmann approximation, also equivalent to neglecting stimulated photon emission,[8] is used to describe both the electron and photon statistics.

H/A is the *view factor* (also called *étendue* or multilinear Langrage invariant) per unit area.[9] The differential element is $dH=n^2 d\varpi \cos\theta dA$, where n is the index of refraction of the medium through which the light is propagating, $d\varpi=\sin\theta d\varphi d\theta$ is the element of solid angle of the bundle of rays entering or exiting the cell face involved, dA is the element of cell surface area, and θ is the angle of the elementary bundle of rays with the cell surface. This element must be integrated over the angular divergence of the bundle of rays involved. Thus, for example, rays coming from the sun, in a cone of angle θ_s normal to the cell surface, have a view factor of $H/A=\pi\sin^2\theta_s$. For luminescent light leaving the cell isotropically, the view factor is $H_f/A=\pi$ for the front

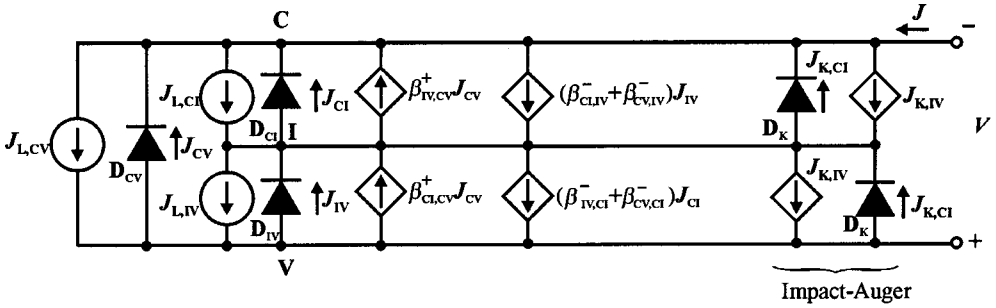

FIG. 2. Equivalent circuit of the IBSC.

TABLE I. Description of the elements that constitute the equivalent circuit of the intermediate band solar cells.

Total contribution to the photocurrent of the transitions from the valence band to the conduction band:

$$J_{L,CV}=eG_{CV}^{\text{ext}}+eG_{EN}+eG_{EP}, \tag{T1}$$

where eG_{EN} is the contribution by the front emitter; eG_{EP} is the contribution by the rear emitter; eG_{CV}^{ext} is the contribution by the intermediate band region

IB to CB photogenerated current:

$$J_{L,CI}=eG_{CI}^{\text{ext}}. \tag{T2}$$

VB to IB photogenerated current:

$$J_{L,IV}=eG_{IV}^{\text{ext}}. \tag{T3}$$

Diodes D_{XY} reverse saturation currents:

$$J_{0,CV}=J_{CV,CV}^{\text{ext}}+J_{0,N}+J_{0,P}, \tag{T4}$$

$$J_{0,CI}=J_{CV,CI}^{\text{ext}}+J_{CI,CI}^{\text{ext}}+J_{JV,CI}^{\text{int}}+en_{eq}W/\tau_C, \tag{T5}$$

$$J_{0,IV}=J_{CV,IV}^{\text{ext}}+J_{CI,IV}^{\text{int}}+J_{IV,IV}^{\text{ext}}+ep_{eq}W/\tau_V, \tag{T6}$$

where $J_{0,N}$, contribution from the recombination in the front emitter; $J_{0,P}$, contribution from the recombination in the rear emitter; $en_{eq}W/\tau_C$, contribution from other nonradiative recombination mechanisms between the CB and the IB; $ep_{eq}W/\tau_V$, contribution from other nonradiative recombination mechanisms between the IB and the CB.

Reverse saturation current for diodes D_K

$$J_{0,K}=ec_Ap_{eq}m_{eq}^2U/A. \tag{T7}$$

Current gain factors:

$$\beta_{a,b}^{\pm}=(J_{a,b}^{\text{int}}\pm J_{c,b}^{\text{ext}})/J_{0,b}, \tag{T8}$$

with a, b, c taking the values CI, IV, or CV

Auxiliary functions:

$$G_{XY}^{\text{ext}}=\int \alpha_{XY}aN_{phl}/(\alpha_{CV}+\alpha_{IV}+\alpha_{CI})d\epsilon,$$

$$J_{a,b}^{\text{int}}=Z_{\text{int}}\int \alpha_a\alpha_b\exp(-\epsilon/kT)\epsilon^2/(\alpha_{CV}+\alpha_{IV}+\alpha_{CI})d\epsilon,$$

$$J_{a,b}^{\text{ext}}=Z_{\text{ext}}\int \frac{(H_f+H_r)a\alpha_a\alpha_b}{(\alpha_{CV}+\alpha_{IV}+\alpha_{CI})^2}\times\exp\left(\frac{-\epsilon}{kT}\right)\epsilon^2d\epsilon.$$

Definitions:

$Z_{\text{int}}=8e\pi n_r^2W/(h^3c^2)$.

$Z_{\text{ext}}=2e/(Ah^3c^2)$.

α_{XY}, absorption coefficient related to optical transitions between band X and Y.

$a=1-\exp[-(\alpha_{CV}+\alpha_{CI}+\alpha_{IV})\zeta]$; absorbance of IB material.

N_{phl}, Spectral photon irradiance in excess of thermal radiation reaching the IB material from illumination external to the IB region.

W, thickness of IB region.

n_r, refraction index of IB material.

h, Planck's constant.

k, Boltzmann's constant.

c, speed of light in vacuum.

e, electron charge.

T, temperature of the cell.

ϵ, photon energy.

A, area of the cell.

$H_{f(r)}$, Étendue of the photons emitted from the front (rear) surface.

p_{eq}, equilibrium hole concentration in VB.

n_{eq}, equilibrium electron concentration in CB.

m_{eq}, equilibrium electron concentration in IB.

τ_C, lifetime associated to other nonradiative recombination mechanisms between the CB and the IB.

τ_V, lifetime associated to other nonradiative recombination mechanisms between the IB and the VB.

c_A, Auger & impact ionization component.

U, Volume of the cell.

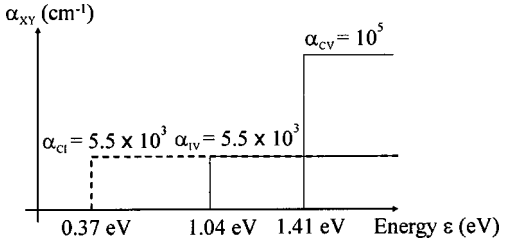

FIG. 3. Simplified absorption coefficients to describe the optical transitions in an IBSC.

face (where the rays escape to the air), and $H_r/A=n^2\pi$ for the rear face (where the rays escape to the semiconductor substrate of refractive index n). In the experimental cells, $H/A=(1+n^2)\pi$.

The complexity of the circuit is due to the fact that some luminescent photons, emitted by the solar cell as a consequence of a radiative recombination mechanism, for example, transitions between the CB and the VB, may be reabsorbed through another kind of transition, for example, between the VB and the IB. In the absence of such transitions, $\beta_{XY,ZW}^{\pm}=0$ and the circuit would greatly be simplified. In addition, if the impact-Auger branches are also neglected, the circuit reverts to the one proposed in Ref. 10.

In addition, the circuit will be further complicated if diodes with ideality factors different from 1 are included in parallel with the existing ones to model, for example, nonradiative recombination phenomena in the space charge regions. This is a trivial generalization of the circuit. Instead, for greater generality to cover other nonradiative recombination phenomena, the lifetimes τ_C and τ_V, and even the emitter recombination terms J_{ON} and J_{OP} are introduced (all fitting parameters, in reality). If necessary, these terms might even be considered nonconstant and dependent on the injection level.

The model involves the absorption coefficients α_{XY} of optical transitions between bands X and Y. Figure 3 illustrates a simplified version of these absorption coefficients that will also be used in subsequent calculations.

The function a is the absorbance of the cell whose value is also given in the Table I. The parameter ζ appearing in it is the average path length of the rays when they travel across the IB region. In most cases it is just W, the thickness of the cell, but in some instances, for example, if the cell surface is textured so that rays are reflected back by total internal reflection it may be much longer,[11] up to $\zeta=4\pi n_r^2WA/H$ where the view factor corresponds to the bundle of luminescent light rays escaping from the cell.

The terms $J_{XY,ZU}^{\text{int}}$ and $J_{XY,ZU}^{\text{ext}}$ in Table I can also be given physical meaning. When a luminescent photon is emitted by the decay of an electron from a higher to a lower energy band—say bands Z and U—it may be reabsorbed producing an upwards transition between the same two bands. Then, both processes cancel out. This takes place in ordinary semiconductors, where only two bands exist, or if the absorption coefficients α_{XY} and α_{ZU} do not overlap. On the contrary, in most IB materials, this photon may be reabsorbed *internally* by transitions between another two bands, say X and Y.

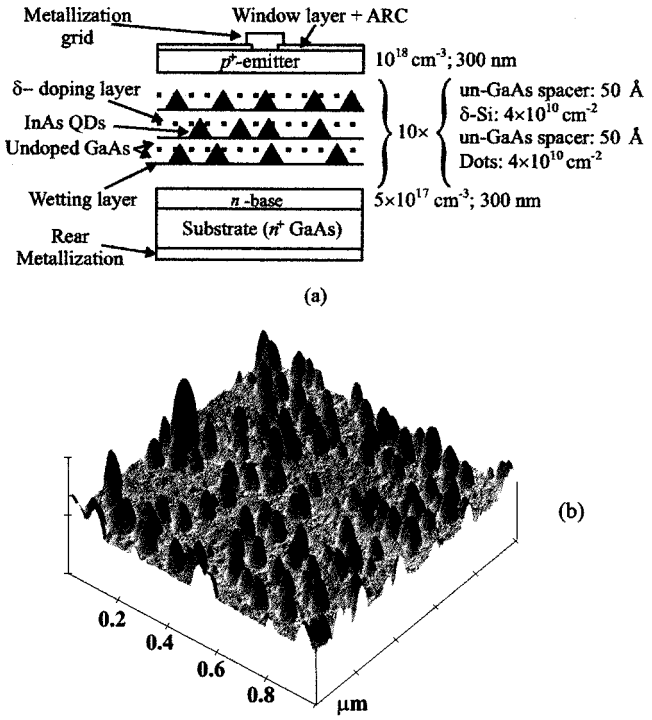

FIG. 4. (a) Prototype of an IB solar cell implemented with InAs quantum dot layers. (b) AFM image of InAs QDs for a sample grown by MBE under conditions similar to those used for the growth of the IBSC structures.

$J^{\text{int}}_{XY,ZU}$ accounts for this mechanism. Terms $J^{\text{int}}_{XY,XY}$ do not appear in Table I because they are self-canceling.

However, photons can escape from the cell (luminescent photons) before reabsorption can take place.

$J^{\text{ext}}_{XY,ZU}$ would then account for them, representing electrons disappearing as radiative recombination from band Z to U that, after being reabsorbed by means of a transition from band Y to X, are effectively emitted to the *exterior* when they recombine back from band X to Y. Therefore, terms of the type $J^{\text{ext}}_{XY,XY}$ are possible.

Finally, the luminescent emission from IB material is characterized by the existence of three main emission peaks, one related to each of the three existing bands and located near the absorption edges represented in Fig. 3. The number

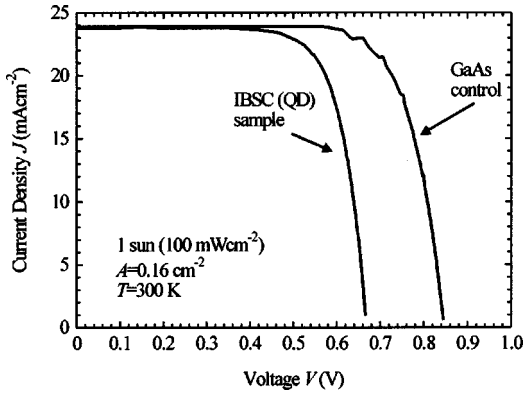

FIG. 5. Current-voltage characteristics under one-sun illumination of an IBSC fabricated from InAs QDs and a GaAs control cell.

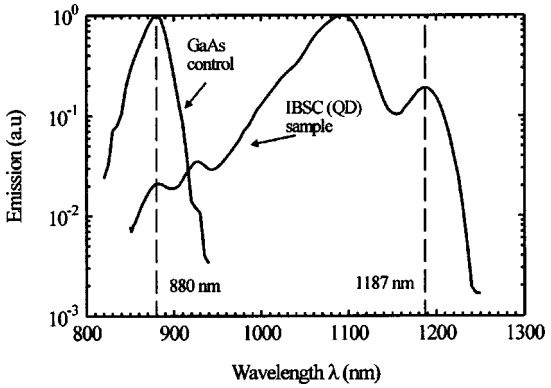

FIG. 6. Electroluminescence spectra obtained with an excitation current density of 5 A cm^{-2} at room temperature.

of photons emitted per unit of time associated with radiative transitions between band X and Y,[6] N^{XY}_{ph} is given by

$$N^{XY}_{ph}=\frac{1}{e}\left(J^{\text{ext}}_{CV,XY}+J^{\text{ext}}_{CI,XY}+J^{\text{ext}}_{IV,XY}\right)\exp\left(\frac{eV_{YX}}{kT}\right). \tag{3}$$

III. APPLICATION OF MODEL TO EXPERIMENTAL DATA

The purpose of this section is to illustrate the application of the equivalent circuit model to experimental devices, in order to obtain both the value of the parameters involved and to gather information about the cell performance.

The structure of the experimental devices is illustrated in Fig. 4(a). The intermediate band[12,13] arises from coupling of the electron energy levels of individual dots. The dots are made of InAs, are embedded in GaAs, and are grown by molecular beam epitaxy (MBE) using the Stranski-Krastanov (S-K) growth mode.[14] The IBSC structure consists of ten quantum dot layers giving a total thickness of 100 nm for the IB region. GaAs solar cells, with identical structure but without the quantum dot layers, have also been fabricated as control cells. Figure 4(b) shows an atomic force microscope (AFM) image of InAs quantum dots (QDs) for a sample grown by MBE under conditions similar to those used for the growth of the IBSC structures.

The circuit model parameters are extracted partly from basic experimental measurements; the current-voltage characteristic, the electroluminescence spectra, and the quantum

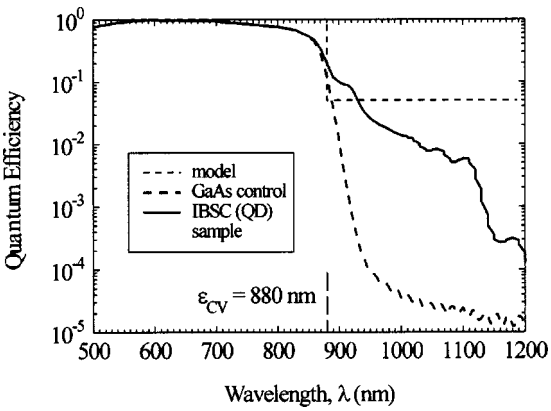

FIG. 7. Quantum efficiency of the GaAs control and IBSC (QD) sample. Results from staircase absorption coefficient model are also shown.

TABLE II. Summary of the data used to obtain the equivalent circuit for the quantum dot intermediate band solar cell prototypes. Cases A and B differ in the value assumed for the absorption coefficient α_{CI}. The radiative case consists of an extrapolation of the QD performance to its radiative limit.

	GaAs control (no QDs)	With QDs (Case A)	With QDs (Case B)	Radiative extrapolation
		Measured values		
J_{SC} (mA cm^{-2})	23.8	24.0		⋯
V_{OC} (V)	0.839	0.666		⋯
$eN_{ph}^{IV}/eN_{ph}^{CV}$	⋯	0.0211		⋯
QE (867–1127 nm)	⋯	0.05		⋯
		Assumed values		
W (nm)	⋯	100		1500
α_{CV} (cm^{-1})	10^5	10^5		10^5
α_{CI} (cm^{-1})	⋯	5.5×10^3	5.5×10^2	5.5×10^3
K_A (A cm^{-2})	⋯	2.3×10^{-18}		3.5×10^{-17}
		Fitting parameters		
$e\int N_{ph1}(\epsilon)d\epsilon$ (mA cm^{-2})@ each range	25	25		25
$J_{0,N}+J_{0,P}$	2.0×10^{-16}	2.0×10^{-16}		0
α_{IV} (cm^{-1})		$5.5\times10^{+3}$	$5.5\times10^{+3}$	$5.5\times10^{+3}$
τ_C (s)		4.0×10^{-9}	4.0×10^{-9}	∞
τ_V (s)		9.5×10^{-12}	9.5×10^{-12}	∞
		Fitting results		
J_{SC} (mA cm^{-2})	25.0	26.28	26.32	35.1
V_{OC} (V)	0.857	0.667	0.665	0.998
$eN_{ph}^{IV}/eN_{ph}^{CV}$	⋯	0.021	0.021	0.054
QE (867–1127 nm)		0.0521	0.0534	0.404
		Quasi-Fermi level split		
eV_{CI} (eV) at $J=5$ A cm^{-2}	⋯	0.154	0.154	0.203
eV_{IV} (eV) at $J=5$ A cm^{-2}	⋯	0.921	0.922	1.188
eV_{CI} (eV) at $V=0$	⋯	2.8×10^{-3}	2.6×10^{-3}	6.8×10^{-2}
eV_{CI} (eV) at $J=0$	⋯	3.1×10^{-2}	3.0×10^{-2}	0.111
eV_{CI} (eV) at $J=0$	⋯	0.668	0.665	0.998

efficiency of the cells (illustrated in Figs. 5–7). The value of other parameters, for example, the GaAs absorption coefficient and some other structural information, has been taken from established data. The complete set of parameters is listed in Table II.

The absorption coefficients are assumed to have the square shape indicated in Fig. 3, and are thus defined by giving their values in the flat regions (α_{CV}, α_{CI}, and α_{IV}) together with the corresponding cut-off energies.

The current-voltage characteristics of both the GaAs control and the IBSC cells are presented in Fig. 5 for one-sun illumination (100 mW cm^{-2}). They have been measured using a xenon solar simulator calibrated against a silicon cell used to set up the one-sun reference illumination level.

The data from the electroluminescence spectra allow the absorption edge of the IB-VB transition ($\lambda_{IV}=1187$ nm or $\epsilon_{IV}=1.04$ eV) and that of the CB-VB transition ($\lambda_{CV}=880$ nm or $\epsilon_{CV}=1.41$ eV, which corresponds also to the band gap of doped GaAs) to be determined. The absorption edge of the CB-IB transition is then taken as the difference between the two ($\epsilon_{CI}=0.37$ eV). These values have also been represented in Fig. 3. For the process that follows of fitting parameters to the circuit elements, a knowledge of this emission in relative units is required. Hence, the fact that the real photon emission towards the rear substrate is n_r^2 times higher than the emission via the front surface becomes irrelevant.

The simplified step-wise absorption coefficients in Fig. 3 also lead to a step-wise quantum efficiency (QE) profile, as shown in Fig. 7. For fitting purposes, a constant averaged quantum efficiency equal to 0.05 has been taken as representative of the cell response in the 867–1127 nm wavelength interval.

The process of extracting the circuit parameters starts with the current-voltage characteristic of the GaAs control cell. Its equivalent circuit is composed only of the current generator $I_{L;CV}$ and the diode D_{CV}. The values of the light intensity and $J_{0N}+J_{0P}$ are tuned until the experimental short-circuit current and open-circuit voltage of the cell are (approximately) obtained. These values are used for the QD cells since it is assumed they are not modified by the introduction of the quantum dots.

The value for α_{IV} is obtained from the QE measurement, particularly from the response of the QD cell in the 880–1197 nm range. It is worth mentioning that, even in the ideal case of nonoverlapping absorption coefficients, current can be extracted from the cell in this wavelength range when performing QE measurements. In this case, the external photon pumps an electron from the VB-IB while thermal radiation, due to the low value of the band gap ϵ_{CI} and the fact diode D_{CI} becomes biased in reverse, suffice to provide the second photon (or, in circuit terms, the reverse saturation current of the diode D_{CI} suffices for not blocking the photogenerated current $I_{L,IV}$). Conversely, α_{CI}, cannot be determined but for most purposes its effect is of minor importance. Therefore, α_{IV} is set to the value required to obtain a QE=0.05 in the wavelength range of interest. For comparison, two different values for α_{CI}: equal to α_{IV} (case A) and 1/10 of α_{IV} (case B) have been selected.

Finally, the values of the lifetimes τ_C and τ_V are chosen to fit simultaneously the open circuit voltage of the QD cell and the $eN_{ph}^{IV}/eN_{ph}^{CV}$ ratio.

The outcomes of the fitting procedure are summarized in Table II. The experimental values are listed first, followed by the fitting parameters described above and finally the results of the fitting. The fitting is found to be good for both two cases A and B.

Under the column labeled ''radiative'' in Table II, the effects of $J_{ON}+J_{OP}$, τ_C and τ_V have been removed. Also, the thickness of the QD region has been enlarged to 150 QD layers (1500 nm), to increase the absorption of light. However, the nonradiative processes associated with kinetic energy transfer, namely, impact ionization and the Auger mechanisms, are retained.

The most important conclusion from Table II is that a split between the CB and IB quasi-Fermi levels does exist.

TABLE III. Values of the circuit elements (currents are in A cm^{-2} and voltages in V).

	Case A		Radiative extrapolation	
Circuit element	Value	Dominant contribution	Value	Dominant contribution
$J_{L,CV}$	2.50×10^{-2}	eG_{EN}	2.50×10^{-2}	eG_{EN}
$J_{L,IV}$	1.32×10^{-3}	eG_{IV}^{ext}	1.01×10^{-2}	eG_{IV}^{ext}
$J_{L,CI}$	2.66×10^{-3}	eG_{CI}^{ext}	2.42×10^{-2}	eG_{CI}^{ext}
$J_{0,CV}$	2.00×10^{-16}	$J_{0,N}+J_{0,P}$	8.86×10^{-21}	J_{CVCV}^{ext}
$J_{0,IV}$	5.58×10^{-13}	$ep_{eq}W/\tau_V$	4.61×10^{-16}	J_{IVIV}^{ext}
$J_{0,CI}$	1.16×10^{-2}	$en_{eq}W/\tau_C$	1.11×10^{-3}	J_{CICI}^{ext}
$\beta_{IV,CV}^{+}$	1.16×10^{-5}	$\beta_{IV,CV}^{+}$	3.44	$\beta_{IV,CV}^{+}$
$\beta_{CI,CV}^{+}$	1.16×10^{-5}	$\beta_{CI,CV}^{+}$	3.44	$\beta_{CI,CV}^{+}$
$\beta_{CV,CI}^{-}+\beta_{IV,CI}^{-}$	1.49×10^{-14}	$(J_{IV,CI}^{\text{int}}-J_{IV,CI}^{\text{ext}})/J_{0,CI}$	2.72×10^{-12}	$(J_{IV,CI}^{\text{int}}-J_{IV,CI}^{\text{ext}})/J_{0,CI}$
$\beta_{CV,IV}^{-}+\beta_{CI,IV}^{-}$	3.09×10^{-4}	$(J_{IV,CI}^{\text{int}}-J_{IV,CI}^{\text{ext}})/J_{0,IV}$	7.66×10^{-1}	$(J_{IV,CI}^{\text{int}}-J_{IV,CI}^{\text{ext}})/J_{0,IV}$
K_A	2.25×10^{-18}	$J_{0,K}$	3.54×10^{-17}	$J_{0,K}$

This justifies the choice of QDs for the implementation of the IBSC concept over quantum well nanostructures. The physical effect that enables this split is known as the phonon bottleneck effect. It is believed to prevent electrons from relaxing quickly from the CB to the confined energy level (band), although it is the subject of much controversy with as many references in favor as against.[15]

Once the fitting parameters have been obtained, it is possible to calculate the value of the circuit elements. The results are shown in Table III for the cases A and ''radiative.'' The dominant component, accounting for at least 99% of the total, is listed. The values of circuit elements that carry at least 1% of the largest branch current are written in boldface.

For case A, the dependent current generators are found to make a small contribution to the circuit currents, so that a circuit with diodes and light dependent generators only provides a good description of the cell. Physically, it also implies that coupling between bands through reabsorption mechanisms is small. In contrast, almost all the circuit branches are necessary for the radiative case.

The impact ionization terms ($J_{K,IV}$ in Fig. 2) play a role in the radiative case under open-circuit conditions. This is deduced by comparing the value of K_A to $J_{0,IV}$. On the other hand, the Auger recombination term, $J_{K,CI}$, plays a negligible role given the low value of K_A compared to $J_{0,CI}$. In case A, none of these kinetic-energy transfer mechanisms plays a noticeable role.

The equivalent circuit for the ''radiative'' case (including the impact-Auger branches) can be used to explore the potential of the present QD IBSCs. It can be shown that an IB solar cell based on the radiative case is characterized by a short-circuit current of 35.08 mA cm^{-2}, an open-circuit voltage of 0.934 V and to a maximum power output at one sun of 27.37 mW cm^{-2}. The GaAs reference cell can also be taken for comparative purposes to its radiative limit. This leads to a short-circuit current of 24.95 mA cm^{-2}, an open-circuit-voltage of 1.098 V and a maximum power output, at one sun of 24.40 mW cm^{-2}.

IV. CONCLUSIONS

Circuit representations of the equations that govern the operation of intermediate band devices have been presented, in which the voltage differences corresponds to the quasi-Fermi level split between bands. The independent current generators represent carrier generation caused by external illumination while the current-dependent ones model coupling between bands due to light reabsorption or impact ionization mechanisms. Diodes represent recombination processes, including those of a nonradiative nature.

The circuit has been used to describe the operation of IBSC prototypes fabricated from InAs quantum dots. Circuit parameters have been obtained by fitting them to experimental data obtained from cell current-voltage characteristics, photon emission spectra, and quantum efficiency or by theoretical calculations.

The analysis of the circuit has revealed evidence that the quasi-Fermi levels of the conduction and intermediate bands are separated, even for the present IB solar cells in which nonradiative recombination processes dominate. This is a very important result because it supports the fundamental theory underlying the operation of the IBSC. In addition, the importance of impact ionization mechanisms compared to radiative ones can be assessed. It is negligible in the prototype cells and small but detrimental in ideal cells of the same materials.

V. ACKNOWLEDGMENTS

This work has been supported by the project FULLSPECTRUM, funded by the European Commission under Contract No. SES6-CT-2003-502620 and the Spanish Plan for R&D (Grant No. TIC2003-02355). L.C. and N.L. are indebted to the Comunidad de Madrid and the UPM, respectively, for financial support. The authors would like to acknowledge careful measurement of the quantum efficiency of the samples by J. L. Balenzategui (CIEMAT).

[1] A. Luque and A. Martí, Phys. Rev. Lett. **78**, 5014 (1997).
[2] A. Luque, A. Martí, and L. Cuadra, IEEE Trans. Electron Devices **48**, 2118 (2001).
[3] S. P. Bremner, C. B. Honsberg, and R. Corkish, in *Proceedings of the 28th IEEE Photovoltaics Specialists Conference*, (IEEE, New York, 2000), pp. 1206–1208.
[4] A. Luque, A. Martí, and L. Cuadra, IEEE Trans. Electron Devices **50**, 447 (2003).
[5] A. Luque and A. Martí, Prog. Photovoltaics **9**, 73 (2001).
[6] L. Cuadra, A. Martí, and A. Luque, IEEE Trans. Electron Devices (To be published).
[7] A. Luque, A. Martí, and L. Cuadra, in *Proceedings of the 16th European Photovoltaic Solar Energy Conference*, edited by H. Scheer, B. McNelis, W. Palz, H. A. Ossenbrink, and P. Helm (James and James, London, 2000), pp. 59–61.
[8] H. C. Casey and M. B. Panish, *Heterostructure lasers: Part A: Fundamental Principles* (Academic, New York, 1978), Chap. 3.
[9] A. Luque, *Solar Cells and Optics for Photovoltaic concentration*, Nonimagining Optics and Static Concentration, edited by A. Luque (Adam Hilguer, Bristol, 1989), p. 308, Chap. 10.
[10] M. A. Green, Prog. Photovoltaics **9**, 137 (2001).
[11] J. C. Miñano, *Physical limitations to Photovoltaic Energy Conversion*, Optical Confinement in Photovoltaics, edited by A. Luque and G. L. Araújo (Adam Hilguer, Bristol, 1990), pp. 50–83.
[12] A. Martí, L. Cuadra, and A. Luque, in *Proceedings of the 28th IEEE Photovoltaics Specialists Conference*, (IEEE, New York, 2000), pp. 940–943.
[13] A. Martí, L. Cuadra, and A. Luque, *Next Generation Photovoltaics: High Efficiency through Full Spectrum Utilization*, Series in Optics and Optoelectronics, edited by A. Martí and A. Luque (Institute of Physics Publishing, Bristol, 2003), pp. 140–162, Chap. 7.
[14] D. Bimberg, M. Grundmann, and N. N. Ledenstov, *Quantum Dot Heterostructures* (Wiley, London, 1999).
[15] A. J. Nozik, *Next Generation Photovoltaics: High Efficiency through Full Spectrum Utilization*, Series in Optics and Optoelectronics, edited by A. Martí and A. Luque (Institute of Physics Publishing, Bristol, 2003), Chap. 9.